Applied Ocean Research 170 (2026) 105069

Contents lists available at ScienceDirect

Applied Ocean Research

journal homepage: www.elsevier.com/locate/apor

Research paper

A coupled LES–aeroacoustic framework for predicting hydrodynamic noise from tidal-stream turbines

Laura Botero-Bolívar [a,*], Pablo Ouro [b,c], Esteban Ferrer [d]

[a] School of Mechanical Engineering, Universidad Industrial de Santander, Energy and Environment Research Group (GIEMA), Carrera 27 calle 95, Bucaramanga, Colombia
[b] Galicia Supercomputing Centre (CESGA), Avenida de Vigo s/n, Santiago de Compostela, 15705, Spain
[c] School of Engineering, The University of Manchester, Oxford Road, Manchester, M13 9PL, UK
[d] ETSIAE-UPM - School of Aeronautics, Universidad Politécnica de Madrid, Plaza Cardenal Cisneros 3, Madrid, E-28040, Spain

ARTICLE INFO

Keywords:
Tidal turbine noise
Amiet's theory
Actuator line
Computational fluid dynamics
Tidal energy
Offshore energy devices

ABSTRACT

A high-fidelity numerical framework is developed to predict the hydrodynamic noise generated by tidal-stream turbines under realistic flow conditions. The approach couples large-eddy simulations (LES) using the actuator-line method (ALM) with Amiet's aeroacoustic theory to quantify underwater sound emissions from turbine blades. The model accounts for both trailing-edge and turbulence-interaction noise sources. Simulations are performed for a full-scale 1 MW, 18 m-diameter tidal turbine operating at various tip-speed ratios and inflow turbulence intensities. The results show that higher tip-speed ratios lead to amplified hydrodynamic noise, while increased turbulence broadens the affected frequency range. Cylindrical sound propagation is applied to represent shallow-water effects, and predictions are extended to a nine-turbine array configuration. The array increases noise levels by up to 8 dB downstream and over 50 dB laterally compared with a single turbine. The coupled LES–Amiet framework provides a computationally efficient and physically consistent method to predict underwater noise from tidal energy devices. These findings improve the understanding of the flow-acoustic coupling mechanisms and support the design and environmental assessment of future marine energy systems.

1. Introduction

The urgent need to decarbonize global energy systems has accelerated interest in marine renewable energy. Among the available technologies, tidal-stream turbines are particularly attractive in regions such as the United Kingdom, Canada, France, and Japan, where there are strong tidal resources (Coles et al., 2021; Garcia Novo and Kyozuka, 2019). Because tidal currents are highly predictable and periodic, tidal-stream turbines provide a reliable and complementary source of renewable power in addition to intermittent wind and solar generation. As deployment efforts increase in both device size and array density, it is essential to assess their potential environmental impacts (Ouro et al., 2024a). An emerging concern is underwater noise, which has been recognized as a widespread anthropogenic pollutant in marine ecosystems (Hemery et al., 2024), with an unknown upscaling when tidal arrays grow in turbine number (Hasselman et al., 2023).

At low frequencies (tens to hundreds of Hz), the marine soundscape is increasingly dominated by human activity, particularly shipping and industrial construction, with average ocean noise levels rising by more than 10 dB since the 1960s (Hildebrand, 2009). Marine species evolved in quieter conditions and rely heavily on sound for essential behaviors: fish use acoustic cues for navigation, habitat selection, and predator avoidance, while marine mammals depend on sound for communication and echolocation (Hildebrand, 2009). Anthropogenic noise can mask these signals and act as a stressor, reducing the effective communication range of vocal animals by 60%–90% in some cases (Pine et al., 2019). Such disturbances can trigger avoidance, increased vigilance, or altered vocalization strategies, with documented consequences for foraging efficiency, navigation, and social interactions (Purser and Radford, 2011; Hastie et al., 2018; Pine et al., 2019). These effects highlight how acoustic pollution can compromise individual fitness and ultimately affect population dynamics.

Tidal turbines add a new source of anthropogenic sound in shelf seas and coastal environments. Field measurements confirm that operating turbines emit strong low-frequency tonal components from machinery and blade–flow interactions, in some cases reaching levels comparable to those of small vessels (Lossent et al., 2018; Risch et al., 2020). Unlike ships or construction activities, which generate transient noise that dissipates as the source moves or ceases, tidal turbines are designed

* Corresponding author.
E-mail address: laura.botero@uis.edu.co (L. Botero-Bolívar).

https://doi.org/10.1016/j.apor.2026.105069
Received 10 November 2025; Received in revised form 17 March 2026; Accepted 13 April 2026
Available online 17 April 2026

to operate continuously for decades, raising concerns about sustained acoustic exposure rather than instantaneous levels. Most energy lies below 1 kHz, although higher frequency peaks (e.g. ~20 kHz) have also been detected closer to operating turbines (Gillespie et al., 2021). The resulting acoustic footprint can extend over kilometers: (Palmer et al., 2021) observed a 64—78% reduction in the presence of harbor porpoise during turbine operation, while playback experiments showed that seals avoided turbine-like sounds up to several hundred meters (Hastie et al., 2018). These responses suggest that turbine noise can act both as a deterrent to collision risk and as a driver of habitat displacement (Sparling et al., 2018; Gillespie et al., 2021). In contrast, small-scale devices may contribute little to background noise; for example, a 25 kW turbine did not produce measurable increases above ambient levels in a high-traffic port (Haxel et al., 2022). However, as turbine capacity and array density increase, cumulative acoustic impacts are expected to become ecologically significant (Hasselman et al., 2023; Lieber et al., 2024).

To quantify these effects, several models have been developed to estimate the spatial and temporal extent of turbine noise. For example, Pine et al. (2019) applied listening space reduction metrics, predicting a > 80% reduction in the acoustic detection range for seals within tens of meters of a turbine. Numerical simulations have also been employed: Lloyd et al. (2014) used large eddy simulations (LES) coupled with the Ffowcs-Williams–Hawkings analogy, identifying leading edge turbulence at blade tips as dominant noise sources. Although their scaled source levels were lower than field measurements — suggesting missing contributions — this work remains one of the few to explicitly link turbine hydrodynamics with acoustic prediction. More broadly, LES and other CFD approaches have been widely used to study turbine wakes and performance (Afgan et al., 2013; Ahmed et al., 2017; Ouro et al., 2017; Ouro and Stoesser, 2019; Posa and Broglia, 2021; Posa et al., 2024; Chawdhary et al., 2018; Zilic de Arcos et al., 2023), but extensions to acoustics remain rare. This scarcity underscores the need for high-fidelity approaches that couple hydrodynamic loading with sound generation.

Here, we address this gap by developing a comprehensive framework that couples high-resolution LES using the actuator line method (ALM) with frequency-domain aeroacoustic modeling to predict hydrodynamic noise from tidal turbines. The LES–ALM solver, DOFAS (Ouro and Stoesser, 2019; Ghobrial et al., 2025), resolves unsteady sectional lift and drag forces under realistic turbulent inflow. These time series are processed with Amiet's trailing- and leading-edge noise formulation (Amiet, 1975; Schlinker and Amiet, 1963) to predict the turbine noise source. The propagation through a layered ocean waveguide model then provides spatial sound pressure level predictions for both individual turbines and arrays. By integrating LES-based hydrodynamics with aeroacoustic modeling, our approach bridges a critical gap in tidal turbine research and enables quantitative evaluation of how turbine design, operating conditions, and environmental factors shape underwater noise signatures.

2. Methods

2.1. Tidal turbine model and operating conditions

To represent a generic three-bladed horizontal-axis tidal turbine, we adopt the widely studied Tidal Generation Ltd. (TGL) DEEPGen IV device as a reference model, as its size, power rating, and design characteristics are representative of full-scale operational turbines currently deployed or planned for commercial tidal energy projects.

The TGL device is a three-blade horizontal axis tidal turbine of 18 m diameter (D) with a nominal power of 1 MW. The main geometric characteristics of the turbine are shown in Table A.1, including radial variation of chord length, airfoil's thickness, pitch angle, and hydrofoil. The turbine is simulated over a range of operating conditions for a constant onset speed U_∞ = 2.5 m/s at the hub height, and for five tip speed ratios (TSR), namely 4.0, 4.5, 5.0, 5.5, and 6.0. The rotational speed is computed as Ω = TSR U_∞/R. The intensity of the inflow turbulence is considered 5.6% with a turbulent integral length scale of about 8 m, obtained during the LES precursor flow. For all conditions, we considered these inflow turbulence values, unless specified otherwise.

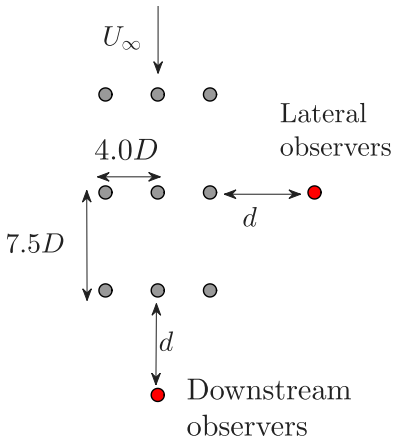

Fig. 1. Layout of the rectangular nine-turbine tidal array, including the two observer locations downstream and on the side of the array.

The cumulative impacts of a set of individual clustered tidal-stream turbines are analyzed by adopting a configuration of the ring. A representative nine-turbine tidal array with rectangular layout with $7.5D$ and $4D$ spacing in the streamwise and spanwise directions, respectively, is considered to predict the noise generated by a group of turbines (Fig. 1). The turbine spacing adopted in the present array configuration is consistent with values commonly considered in tidal farm layout studies. Previous experimental and numerical investigations have shown that streamwise spacings of approximately 6–8D and lateral spacings of about 4–5D provide a compromise between turbine density and wake recovery within the array (Churchfield et al., 2013; Mycek et al., 2014; Ouro et al., 2019). These distances are sufficiently large to allow partial recovery of turbine wakes while still representing realistic packing densities in tidal energy farms. The spacing values selected in this study ($7.5D$ streamwise and $4D$ lateral) therefore fall within the typical range reported in the literature. It is worth noting that the objective of the present work is not to optimize the array layout but rather to adopt a representative configuration to investigate how the acoustic emissions of a single turbine may scale when multiple devices operate within an array.

It should be noted that the purpose of this configuration is to provide a first-order estimate of how the acoustic emissions from a single turbine may scale when multiple devices operate within an array. The acoustic field of the array is therefore represented as the superposition of the contributions from nine turbines located at the prescribed positions. This approach assumes identical operating conditions for all turbines and neglects detailed wake–wake interactions and potential modifications of the inflow turbulence between turbines. While these effects may influence the hydrodynamic and acoustic response in real deployments, their accurate representation would require fully coupled simulations of the entire array. The present approach instead aims to provide a computationally efficient framework to approximate the cumulative acoustic footprint of a tidal turbine array and to investigate how the spatial distribution and directivity of turbine noise may expand the potential detection region when multiple sources are present.

The adopted coordinate system is located in the center of the turbine rotor hub, where x is in the flow direction, y is the horizontal direction pointing to the left, and z is the vertical direction pointing upstream.

2.2. Large-eddy simulation setup

High-fidelity numerical simulations of the 1 MW TGL turbine (Scarlett et al., 2019) are performed using the fully parameterized in-house code DOFAS that solves the spatially filtered Navier–Stokes equations for incompressible and viscous flows. DOFAS has been validated in several studies for tidal turbine flows, including surface waves (Ouro et al., 2024b; Christou et al., 2025), irregular bathymetry (Ouro and Stoesser, 2019; Hurubi et al., 2025) and farms (Ouro and Nishino, 2021; Ouro et al., 2023), as well as for wind energy (Ghobrial et al., 2025) or turbulent hydraulic flow applications (Liu et al., 2024). DOFAS features an actuator line method (ALM) with a Gaussian interpolation function for velocity and force interpolation between the ALM markers and the fluid grid cells (Ouro et al., 2019). The current ALM adopts a tip-loss correction similar to Shen et al. (2005). The turbine nacelle is modeled using a direct-forcing immersed boundary method, whereas the support structure is not taken into consideration in the LES. The WALE sub-grid scale model (Nicoud and Ducros, 1999) is adopted in the current LES setup.

The rectangular computational domain measures 576 m×576 m in the horizontal dimension and a water depth of 42.2 m is adopted as representative of the EMEC site in Scotland (UK) where this turbine operated (Sellar et al., 2018). The turbine is located at 139 m in the streamwise direction and 300 m in the lateral direction, with a hub height of 15.2 m. The free surface is treated as a lid with shear-free boundary conditions without explicit deformation of the water surface, which has been demonstrated that with the clearance on the tip does not affect the flow field around the turbine (Ouro et al., 2024b, 2022). The boundary conditions on the lateral sides are slip and on the bottom surface a smooth wall is assumed. Before the turbine simulation, bare-flume precursor simulations are performed to obtain fully developed turbulent conditions. The results of the spatially and temporally averaged precursor flow show a hub height flow speed of about 2.5 m/s with a rotor-averaged turbulence intensity of 5.6%. Then, cross-sectional planes of instantaneous velocities are extracted to drive the turbine simulation. In both the precursor and concurrent simulations, a fixed time step of 0.015 s and a uniform grid resolution of 0.32 m were used, providing a total of 56 grid points across the turbine diameter, which is sufficient for the resolution required by the actuator line method (ALM) (Troldborg et al., 2011). The total number of grid cells is 114 million and simulations are run using 200 CPUs to cover a total simulation time of 40 turbine revolutions with mean blade hydrodynamic statistics collected over the last 20 revolutions. Validation of the LES–ALM solver with reference BEMT data is provided in Appendix B in terms of power (C_P) and thrust (C_T) coefficients for two mesh sizes and comparison with reference data.

2.3. Noise prediction method

Noise predictions assume turbulence-interaction noise (also known as leading-edge noise) and trailing-edge noise as unique noise sources. We compute tidal turbine noise using the Amiet–Schlinker method for rotatory noise sources (Schlinker and Amiet, 1981), where the relative motion of the segment that induces a delay between noise emission and the location of the observer is considered using the Doppler effect. The total turbine noise is calculated using the strip theory approach, where the blade is divided into n segments that produce uncorrelated noise. n is defined as the maximum number of segments such that each segment has an aspect ratio (span over mean section chord) larger than 3 to guarantee the far-field noise condition needed in Amiet's theory. Therefore, each segment is treated as a 2D airfoil, for which turbulence interaction noise and trailing-edge noise are computed using Amiet's theory (Amiet, 1975, 1976). Subsequently, the blade noise is calculated as the sum of all segments at every angular position. The total hydrodynamic noise produced by the tidal turbine is computed as the integral of the total blade noise at each azimuth angle over one rotation, considering the same contribution from the three blades of the modeled TGL turbine. A detailed description of the noise prediction approach is reported in Botero-Bolívar et al. (2024). This paper also validates noise prediction method by comparing predicted noise spectra using actuator line coupled with Amiet's theory with field-measurements.

It is worth noting that alternative aeroacoustic approaches based on large-eddy simulations coupled with the Ffowcs Williams–Hawkings (FWH) acoustic analogy could also be used to predict turbine noise. However, such approaches require resolving the near-wall boundary layers and performing highly time-resolved simulations capable of capturing the high-frequency acoustic content of the sources. For rotating machines such as tidal turbines, this leads to a very high computational cost, particularly when multiple turbines are considered. In contrast, the present approach combines detailed hydrodynamic information obtained from LES with the analytical Amiet formulation for turbulence-interaction and trailing-edge noise. This hybrid framework significantly reduces the computational burden while retaining the essential flow physics responsible for sound generation. As a result, the methodology enables efficient exploration of different operating conditions and turbine configurations, including simplified representations of tidal turbine arrays, which would be computationally prohibitive to simulate using full-geometry LES–FWH approaches.

The input for the prediction of the noise of the turbulence interaction is the turbulence spectrum, which is computed with the von Kárman spectrum, using as input the turbulence intensity of the oncoming flow (Tu_∞) and the integral length scale of the ambient turbulent (L). The predictions are computed with $Tu_\infty = 5.6\%$, and L =8 m, based on the results obtained from the precursor large-eddy simulations. For trailing-edge noise prediction, the inputs for Amiet's theory are the WPS, which is computed with the TNO-Blake model, which is based on the solution of the Poisson equation, and the spanwise correlation length, which is computed using Corco's method (Corcos, 1964). To calculate the WPS, the input needed is the angle of attack and apparent velocity at every blade segment or ALM point in the current case, which are used to perform XFOIL simulations to extract the boundary layer parameters (δ, δ^*, θ, and τ_w). The transition for XFOIL simulations was forced at $x/c = 0.01$.

In noise prediction, the blades are divided into six segments, keeping the aspect ratio of each segment larger than 3. Additionally, 10 azimuthal locations are used to predict the noise over one rotation.

For a single turbine, observers are deemed to be located downstream of the turbine at the hub height and aligned with the flow direction. For instance, an observer located at $5D$ downstream, with D being the turbine's diameter, the observer's coordinates are: ($5D$,0,0). For the prediction of the noise of the nine-turbine tidal array, a global observer is defined, that is, downstream and lateral, with the distance measured from the last turbine of the array (Fig. 1).

In shallow water conditions, representative of the tidal flows in which tidal turbines are deployed, the sound propagates following a cylindrical propagation, i.e., with d instead of d^2 characteristic of free fields, where d is the distance from the noise source (the tidal turbine) and the observer. This is considered in this research by rescaling the noise of the tidal turbine to the noise source with d^2 and propagating again to the observer with d. Additionally, the attenuation of sound underwater is calculated for each segment at each azimuth location as: $A_w = \alpha_w d$, where α_w is the sea-water attenuation in dB/m, calculated as proposed by Fisher and Simmons (1977). Noise level is finally calculated as:

$$L_p = L_{p|predicted} + 20\log_{10} d - 10\log_{10} d - A_w; \quad (1)$$

where $L_{p|predicted}$ is the noise predicted by the model. For the tidal array, this rescaling is performed for each turbine.

The noise prediction method used in this study is based on analytical and semi-analytical formulations that are firmly established in aeroacoustics and naturally extend to underwater applications. The validity of this approach is not only theoretical but also demonstrated in a wide

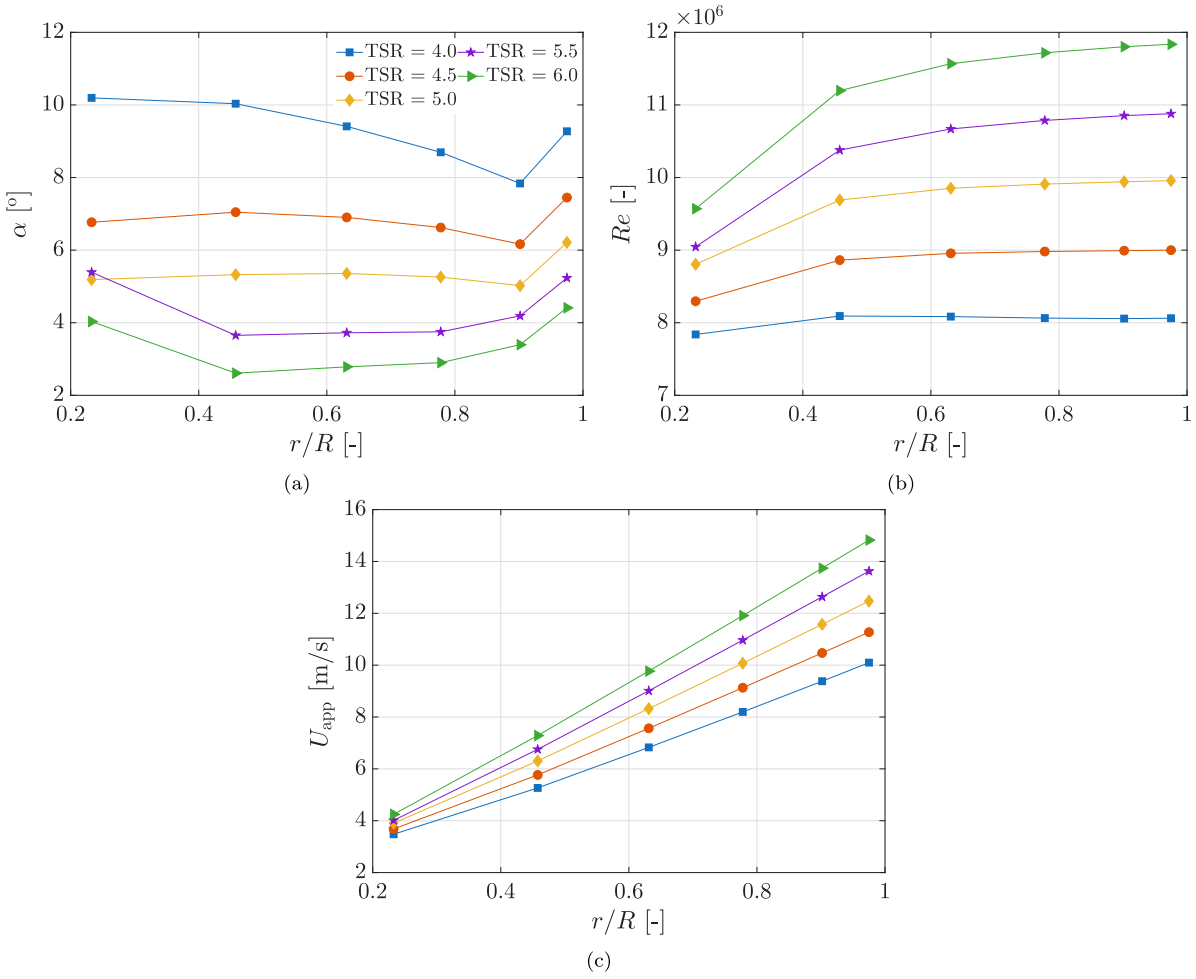

Fig. 2. Radial variation of (a) angle of attack α, (b) chord-based Reynolds number Re, and (c) apparent velocity U_{app}, for several turbine operational conditions obtained from the LES–ALM results and used in the acoustic noise calculation.

range of previous studies, where Amiet's theory and related methods have been successfully used to model underwater noise sources such as marine propellers (Dos Santos, 2023; Choi et al., 2021; Go et al., 2023; Kim and Kinnas, 2022; Nigro and Abrahams, 2016).

2.4. Hearing threshold of marine animals

The hearing threshold of animals refers to the quietest sound intensity that an animal can detect. It is the minimum level of sound pressure that causes a response in the animal's auditory system. The threshold varies across species and can depend on factors like frequency range and environmental conditions. Different animals have different hearing thresholds, with some being sensitive to higher or lower frequencies than others (United States. National Marine Fisheries Service. Office of Protected Resources, 2024). The hearing threshold of animals is typically determined by audiometric testing, which involves presenting sounds of varying frequencies and intensities to the animal and measuring its response. When marine animals are exposed to sound that is much louder than the hearing threshold, they can experience a Temporary threshold shift (TTS), that is a temporary, reversible increase in the threshold of audibility at a specified frequency, Auditory injury (AUD INJ), that is a damage to the inner ear, and a Permanent threshold shift (PTS), that is a permanent, irreversible increase in the threshold of audibility at a specified frequency (United States. National Marine Fisheries Service. Office of Protected Resources, 2024).

The hearing thresholds presented in this study are derived from publicly available data in the literature. Conducting audiometric measurements across different species is beyond the scope of this research. Tougaard (2021), Southall et al. (2019) compiled various reported hearing thresholds for cetaceans, pinnipeds, and harbor seals, classifying these species into four functional hearing groups: low-frequency (LF), high-frequency (HF), very-high-frequency (VHF), and Phocid pinniped (PCW). Using experimental data, they derived empirical functions to estimate the hearing thresholds for each functional group.

For other species, hearing threshold data are directly sourced from previously published measurements: salmon (Harding et al., 2016), sharks (Nieder, 2023), Atlantic herring (Enger, 1967), and Atlantic cod (Hawkins and Popper, 2020).

3. Results

This section presents the results of the far-field noise prediction for several turbine operating conditions and at several observer locations, considering a single tidal turbine and an array of nine turbines. Far-field noise spectra are compared with the hearing threshold (HT) of several animals. A hearing threshold is defined as the minimum noise level that a species can hear at any frequency. Therefore, when the noise level of the tidal turbine or array (L_p) is higher than the hearing threshold (HT) of the target species, the operating turbines can be heard by the animal. The disturbance in animal life caused by the noise from the tidal turbine depends on the difference between the noise

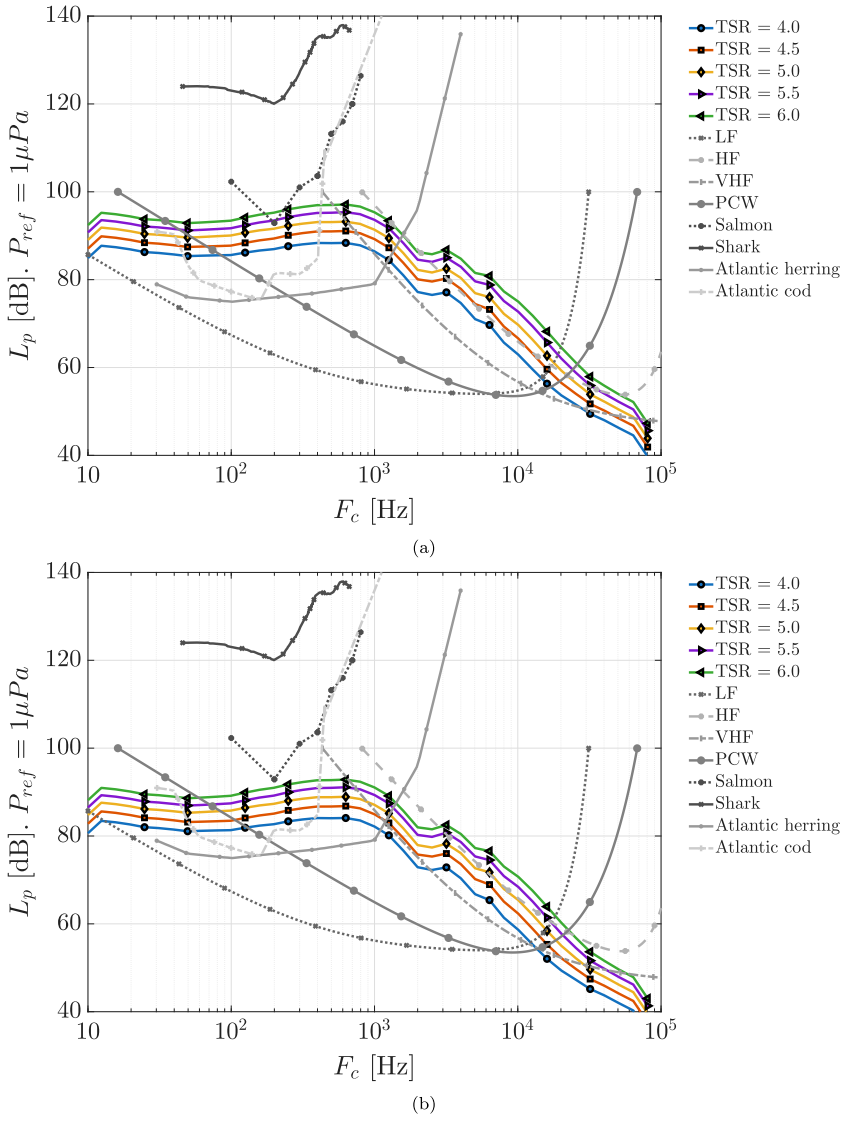

Fig. 3. Single turbine: Far-field noise prediction at (a) $5D$ and (b) $30D$ downstream of the device at hub height during the operation of a single tidal turbine at several operational conditions, together with data from relevant fish and marine mammal species.

of the turbine and the hearing threshold at the frequency where the animal has greater sensitivity (Southall et al., 2019). However, a full assessment of the behavioral and ecological consequences is beyond the scope of this study.

In consultation with leading tidal energy project developers and policy bodies, the following species are included in the present analysis due to their relevance in the development of tidal projects in the UK and France, namely: Salmon, shark, Atlantic herring, and Atlantic cod. In addition, some functional hearing groups are also used for completeness. Low-frequency (cetaceans) refers to Mysticete whales, including minke whale; high-frequency (cetaceans) includes most odontocetes, white-beaked dolphins, and pilot whales. Very high-frequency (cetaceans) groups narrow-band high-frequency odontocetes and harbor porpoise. Finally, pinnipeds (phocid seals) include true seals, harbor seal, and gray seal.

3.1. Operational conditions

In this section, the noise produced by a single tidal turbine is predicted under several operational conditions. When the operational condition of the tidal turbine changes in terms of tip-speed ratio due to variations in the rotational speed or inflow speed, the hydrodynamic loading over the turbine's blade varies. All of these conditions have a direct effect on the noise produced by the tidal turbine. Therefore, in the first part of the results, we will show how the noise source is changed for the several operational conditions analyzed. Later, the far-field noise spectra are shown.

3.1.1. Noise source

In this study, we modeled the two dominant noise sources of a tidal turbine: leading-edge (LE) and trailing-edge (TE) noise, both of which arise during turbine operation. We investigate how the tip-speed ratio (TSR) influences the blade operating characteristics, which in turn govern LE and TE noise generation. In other words, TSR affects noise indirectly through its impact on blade loading and apparent velocity. Fig. 2 shows the distribution along the blades of the key parameters governing noise generation: the angle of attack, the Reynolds number based on the blade-section chord, and the apparent velocity. The angle of attack and Reynolds number provide useful indicators of boundary layer state in each airfoil section, although the direct response also depends on the geometry of the airfoil, as accounted for in the simulations of XFOIL (Drela, 1989). Among these factors, the apparent (or total) velocity at the blade section is particularly important for noise

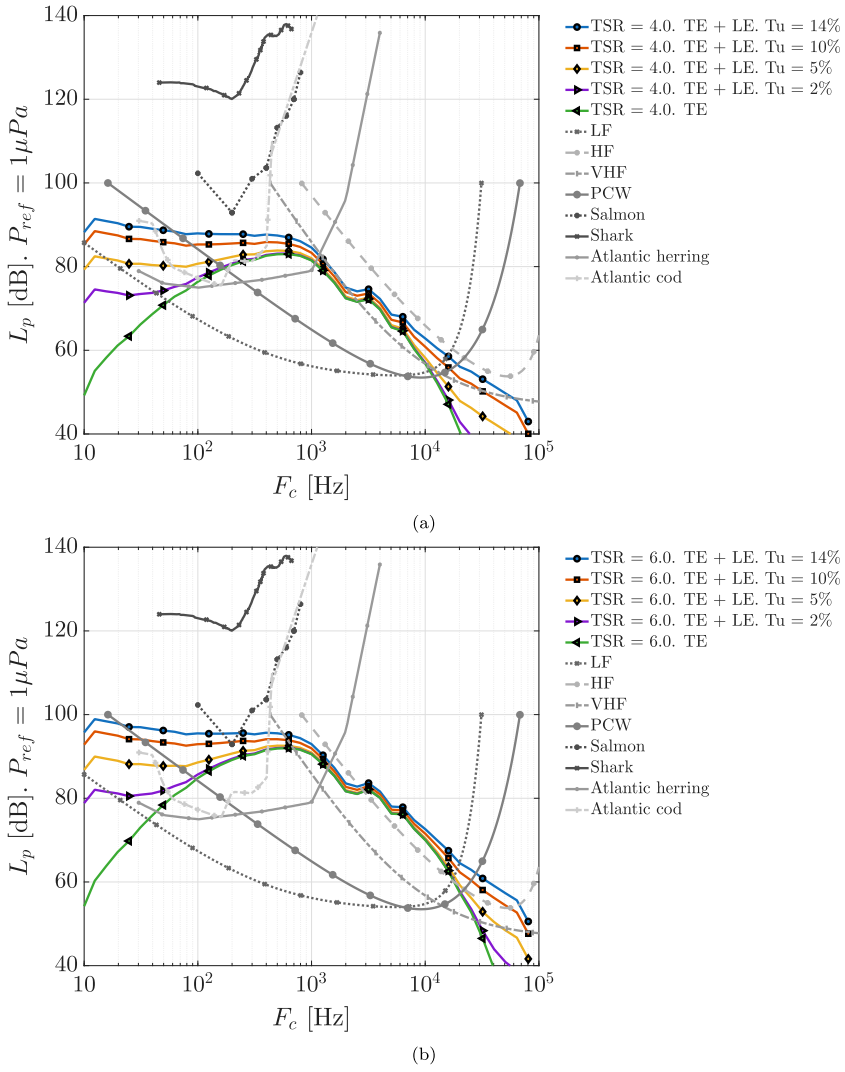

Fig. 4. Single turbine: Effect of the inflow turbulence and noise source on the far-field noise for cases with the turbine operating at a TSR of 4.0 (a) and 6.0 (b). Observer is at 30D downstream of the turbine aligned with the turbine's center and at hub height.

prediction, since both LE and TE noise scale with the Mach number to the fifth power.

The variation of the operational conditions analyzed is based on varying the tip-speed ratio (TSR), which is due to an increase in the rotational speed of the turbine while the inflow velocity remains constant. When the rotational speed is increased or decreased, the hydrodynamic load of the blade varies with the peak performance for this TGL turbine attained at a TSR of 5.5. Hence, operating above that TSR leads to a reduction in the peak power coefficient but reduces the angle of attack on the blade (Fig. 2a), which has advantages to avoid stall during adverse wave conditions, for example. In contrast, when the turbine operates below its nominal TSR, the angle of attack increases and thus the potential for flow separation with a decrease in apparent velocity (Fig. 2c). Fig. 2a shows that the variation in the angle of attack is not linearly related to the variation in the TSR. Regarding noise generation, having a lower angle of attack (higher TSR) is a positive outcome, since, as a general trend, lower angles of attack produce lower and higher frequency trailing-edge noise. It is important to note that low-frequency noise is usually more critical than high-frequency noise because sound waves propagate over longer distances as they have larger wavelengths; moreover, in water, acoustic attenuation increases with frequency, meaning that high-frequency noise is absorbed more rapidly and therefore does not travel as far (Hansen et al., 2017). However, this positive effect of reducing the angle of attack is countered by the negative effect of the apparent velocity discussed later, since the noise from LE and TE scales with the velocity in the power of fifth.

The Reynolds number based on the local chord length (Fig. 2b) follows a similar trend for all operating conditions with only a vertical shift. This is because the only change is the apparent velocity (Fig. 2c) while the blade geometry remains constant. The effect of the Reynolds number on trailing edge noise is not straightforwardly analyzed. Higher Reynolds numbers usually produce higher frequency noise because of the smaller thickness of the boundary layer. Botero-Bolívar et al. (2023) experimentally showed that the trailing-edge noise level scales with the Reynolds number in a power of three, while the frequency scales with Re^{-1}. The apparent velocity follows a linear increase with the radial position, since the resultant velocity is almost dominated by the rotational speed. As the TSR increases, the velocity increases. The slightly different slope for each TSR is caused by the difference in the induced velocity that is related to the angle of attack.

3.1.2. Far-field noise

In this section, we discuss the hydrodynamic noise produced by a single turbine. The noise is predicted using Amiet's theory,

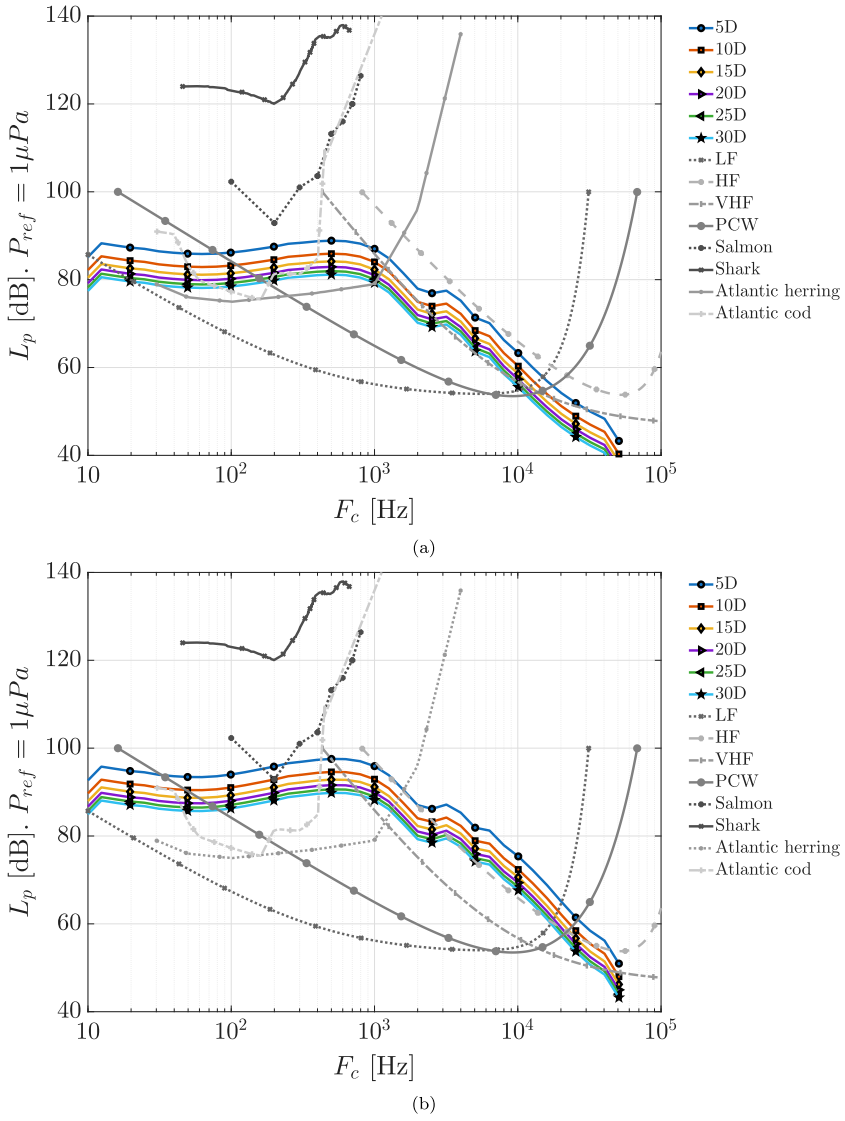

Fig. 5. Single turbine: Far-field noise produced by a single tidal turbine operating at a TSR of (a) 4.0 and (b) 6.0, evaluated at several distances downstream aligned with the turbine's center and at hub height.

coupled with a cylindrical propagation and underwater noise absorption, as is explained in Section 2.3. Far-field noise is compared with the hearing threshold of several marine species, i.e., low-frequency (LF), high-frequency (HF), very-high-frequency (VHF) and Phocid pinniped (PCW), Salmon, Shark, Atlantic herring, and Atlantic cod, see Section 2.4 for information about the hearing thresholds.

Fig. 3 shows the far-field noise spectra at two observers located at $5D$ and $30D$ downstream of the turbine. Results show that at higher TSRs, the footprint in the far-field noise increases for all frequencies. The influence of TSR is consistent at both downstream distances, as the noise originates from the same source. Closer to the tidal turbine, at $5D$ downstream, its noise affects almost all the species considered here, except the shark, which has a much larger hearing threshold. Furthermore, salmon are almost not affected, since the noise from the tidal turbine is only slightly higher than its hearing threshold in a narrow frequency range around $1 - 3 \cdot 10^2$ Hz, only when TSR > 5.5 and close enough to the turbine, i.e., closer than 90 m ($5D$). It is observed that at $30D$ downstream of the turbine, salmon are not affected (Fig. 3b). For the investigated turbine and operational conditions, the most critical species are low- and very high-frequency hearing groups, namely Atlantic herring and Atlantic cod, since they can hear a single turbine at all operational conditions even when they are more than 540 m ($30D$) downstream of the turbine.

A particular condition that significantly affects leading-edge noise is inflow turbulence. The effect of the inflow turbulence in the far-field noise spectrum is shown in Fig. 4 for TSR equal to 4 and 6 evaluated at $30D$ downstream of the turbine. The turbulence intensity (Tu) ranged from 2% to 14%, while in the precursor LES Tu is equal to 5.6%. When inflow turbulence is not considered, i.e., uniform inflow, leading edge noise is not generated, and thus, trailing edge noise is the only noise source. Results show that even with a low turbulence intensity of 2% noise amplitude increases at low frequencies (Fig. 4).

For both TSRs, a similar impact of increasing turbulence intensity is observed with an increase in the low- and high-frequency ranges, while there is a similar noise footprint in the frequency range of 1–10 kHz. This range is where trailing-edge noise has a greater impact on this specific turbine. The trailing edge noise for a two-dimensional airfoil has a maximum at $St = f\delta/U \approx 0.3$, where δ is the thickness of the boundary layer. Combining the effect of all sections at every azimuthal position results in TE noise being louder at $f = 650$ Hz.

In general, higher turbulence intensity in the onset flow broadens the frequency range over which marine species are affected, primarily because of increasing noise levels at lower frequencies. At the same

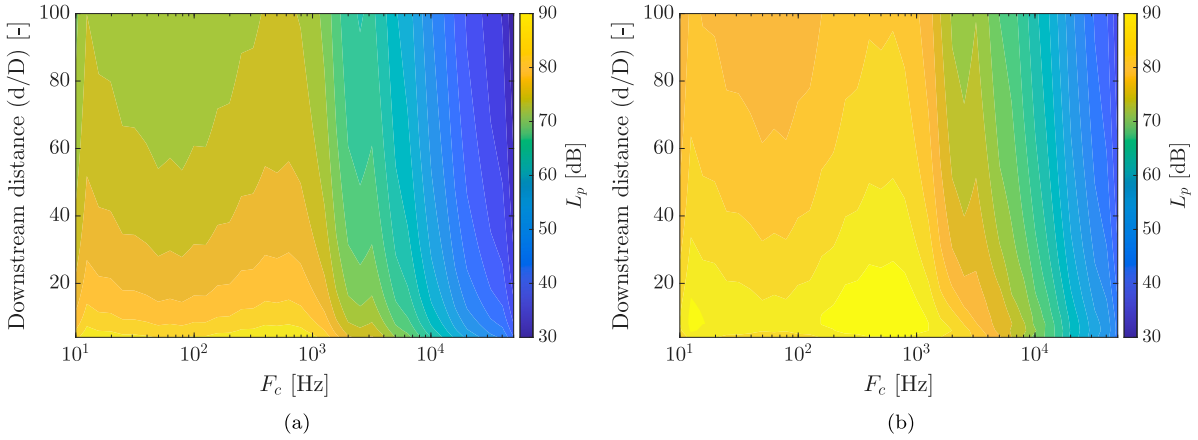

Fig. 6. Single turbine: One-third sound pressure level contour as a function of the distance and frequency. *y*-axis is the downstream distance in terms of the turbine diameter. (a) TSR = 4.0 and (b) TSR = 6.0.

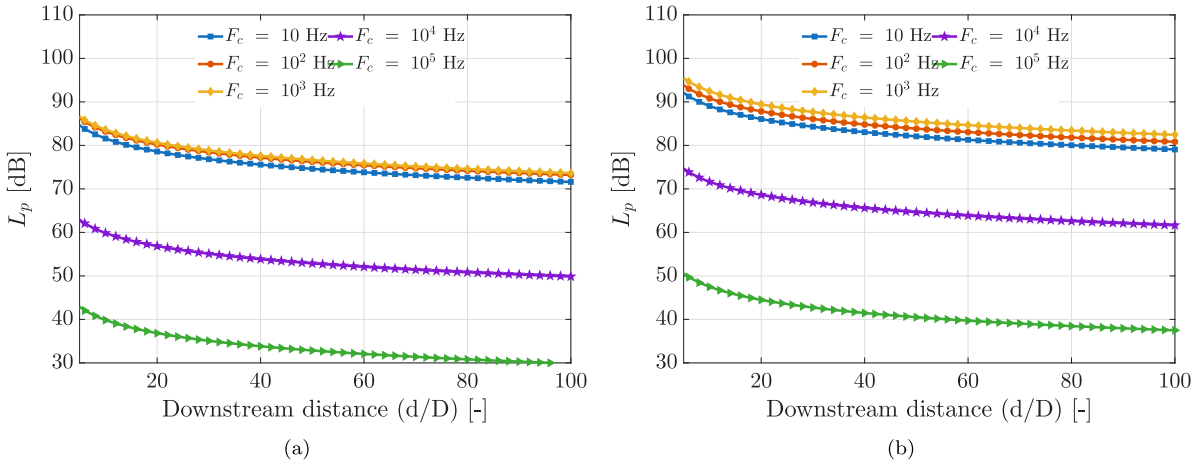

Fig. 7. Single turbine: Far-field noise prediction at several downstream distances from 4D to 100D for several specific frequencies. *x*-axis is the distance in terms of the turbine diameter. (a) TSR = 4.0 and (b) TSR = 6.0.

time, higher turbulence reduces the distance from the turbine at which animals experience detectable noise levels. This effect is particularly relevant for salmon: for example, at TSR = 6.0 and under uniform inflow conditions (where only TE noise is present), salmon are not affected by turbine noise. However, when the inflow turbulence intensity exceeds ≈ 10%, salmon begin to experience detectable noise impacts (Fig. 4b).

At sites candidate for tidal array projects, the environmental flow in which the tidal turbines are characterized by mid to high turbulence intensities, typically ranging between 5% and almost 20% (Garcia Novo and Kyozuka, 2019; Milne et al., 2016). Therefore, LE noise should be considered when estimating the acoustic impact of tidal turbines. However, higher turbulence intensities are developed when tidal velocities are lower, which can condition the operating point of the turbine and last for short time intervals.

3.2. Noise propagation - Effect of distance

Fig. 5 shows the noise spectra calculated at various downstream distances from 5D to 30D when the turbine operates at a TSR of 4 and 6. A tidal turbine radiates noise as a dipole aligned with the inflow velocity (Schlinker and Amiet, 1963); therefore, analyzing the propagation of noise downstream is an appropriate approach to estimate the distance at which the noise of the tidal turbine becomes relevant for specific species. For both TSR and at all distances considered, low- and very high-frequency cetaceans, pinnipeds, Atlantic herring, and Atlantic cod are affected by a single turbine. The specific frequency range depends on the TSR and distance, following the trend that noise is higher for higher TSR and closer to the turbine. In particular, high-frequency cetaceans hear the turbine up to 30D downstream for TSR = 6.0, but remain unaffected for TSR = 4.0. Furthermore, salmon are slightly affected when the turbine operates at TSR = 6.0 for distances less than 10D.

Contours of the one-third noise level as a function of the downstream distance and frequency are presented in Fig. 6 for TSR = 4.0 and 6.0. The maximum noise level along the frequency range is slightly moved towards higher frequencies for higher TSR. These results show that when the turbine operates at TSR = 6.0 the far-field noise is higher than 80 dB for frequencies lower than 1 kHz even at 80D downstream (i.e., more than 700 m). For completeness, Fig. 7 presents the decay of the far-field noise level as a function of the downstream distance for several specific frequencies, up the maximum downstream distance of 100D (i.e., 1800 m). Far-field noise decays with the downstream distance roughly proportional to $10\log_{10}$ for the entire frequency range, as can be observed from the curves in Fig. 7.

3.3. Acoustic exposure zones

In this section, we combine the noise predictions with audiograms of marine species to quantify the extent of the audible zones surrounding

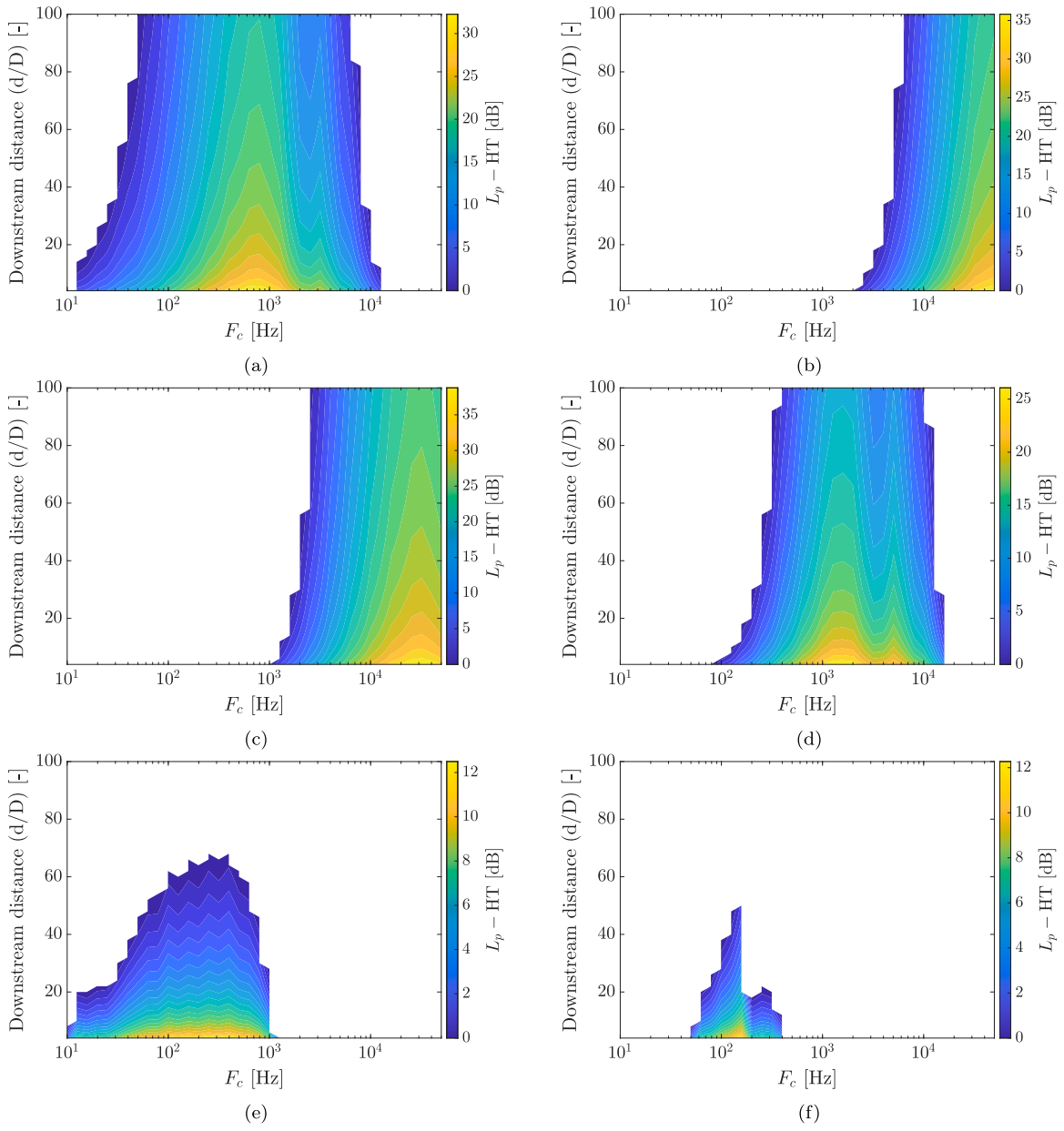

Fig. 8. Single turbine at TSR = 6.0: Contour plots showing the predicted auditory detection range of the most critical marine species as a function of distance and frequency. The color contours represent the difference (in dB) between the predicted sound pressure levels from the tidal turbine at specific distances and frequencies and the corresponding hearing threshold at that frequency. y-axis is the distance in terms of the turbine diameter downstream at the hub height. (a) Low-frequency hearing functional group. (b) High-frequency hearing functional group. (c) Very High-frequency hearing functional group. (d) Pinnipeds. (e) Atlantic Herring. (f) Atlantic cod.

the turbine wake region. Considering the single turbine operating at TSR = 6.0, Fig. 8 presents the regions predicted to be audible as a function of sound frequency (F_c, horizontal axis) and the downstream distance normalized by the diameter of the turbine (vertical axis), relative to various marine species, namely low-, high-, and very high-frequency hearing functional groups, pinnipeds, Atlantic Herring, and Atlantic cod. The colored contours represent the difference between the noise level of the turbine and the hearing threshold of each species group. Warmer colors indicate larger differences, with the scale ranging from zero (threshold of audibility) to the maximum value observed for that species. Contours are presented from 4 to 100 D downstream of the turbine and across the frequency range of 10 to 50 kHz. Blank areas correspond to regions where turbine noise falls below the hearing threshold and therefore is not perceived by that species.

Importantly, these contours indicate both where turbine noise is detectable by marine animals and where it is unheard for certain species. Such zones may present an increased risk of collision as the turbine does not provide an audible signal of its presence. Beyond collision risk, comparing turbine noise with hearing thresholds also helps identify regions of potential impact: where the sound is just audible, where it may interfere with communication through masking, where it could trigger behavioral responses, and, at sufficiently high levels, where it may cause hearing damage. However, exact thresholds for these effects vary between species and depend on how far above the hearing threshold the turbine noise occurs (Erbe and Thomas, 2022).

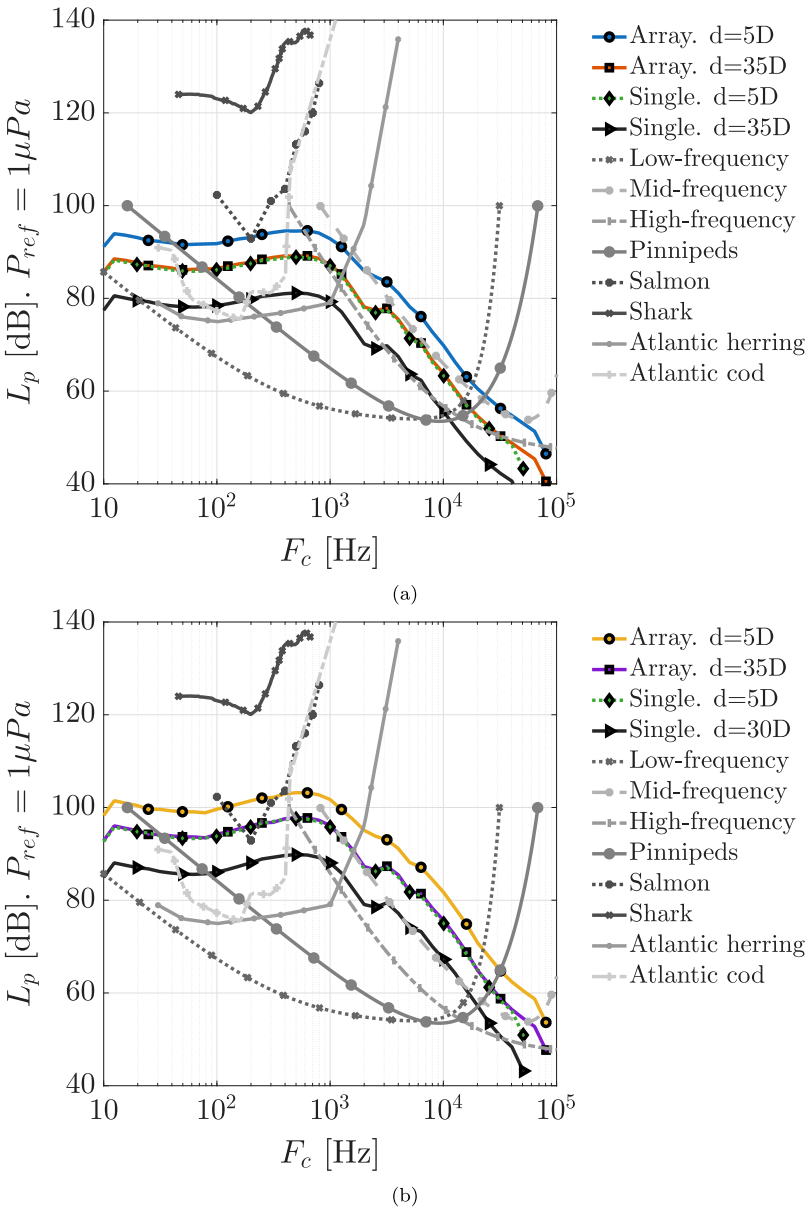

Fig. 9. Tidal array: noise of a rectangular layout of nine turbines evaluated at a distance d downstream the last central turbine (Fig. 1). (a) TSR = 4.0 and (b) TSR = 6.0.

3.4. Tidal array noise

We calculate the noise produced by a compact rectangular array of nine tidal turbines. Noise is predicted at four observer locations, two downstream and two lateral (see Fig. 1 for the definition of the layout and observers' locations) and for two operational conditions, i.e., TSR = 4.0 and 6.0. For all cases, the noise of the tidal array is compared with the noise produced by a single turbine at the same observer, i.e., an observer located at a distance d downstream and in the rotor plane. Fig. 9 shows the far-field predicted noise of a tidal array for downstream observers, and Fig. 10 shows the far-field noise for lateral observers.

For downstream observers (Fig. 9), the increase in the far-field noise of the tidal array, compared to a single turbine, is almost constant throughout the frequency range. For a $5D$ distance downstream, the increase is approx. 6 dB, whereas for a distance of $35D$ the increase is about 8 dB for both TSR along the entire frequency range. The presence of this tidal array is particularly crucial for salmon and the high-frequency hearing group, as they are mostly unaffected by a single turbine, but the array does perturb them, i.e., noise is higher than the hearing threshold.

For lateral observers (Fig. 10), the tidal array significantly increases propagated noise compared to a single turbine. It was mentioned before (Section 3.1.2) that a single tidal turbine radiates noise as a dipole aligned with the inflow. This means that in the rotor plane, for lateral observers, the noise radiated by a single turbine is minimal. In fact, in the rotor plane, a single turbine produces a far-field noise that is much lower than the hearing threshold of the marine animals considered in this research, i.e., more than 20 dB lower. For the tidal array, the far-field noise is louder than 50 dB compared to a single turbine. This increase is explained by the fact that the lateral observers are in the plane of the minimal noise radiation of a unique turbine, whereas for the other turbines the global observer is in a different direction. Furthermore, in the lateral direction, as d increases, the global observer is closer to the direction of lower noise radiation for other turbines. This explains why the difference between the observer at $d = 5D$ and $30D$ is greater for low frequencies.

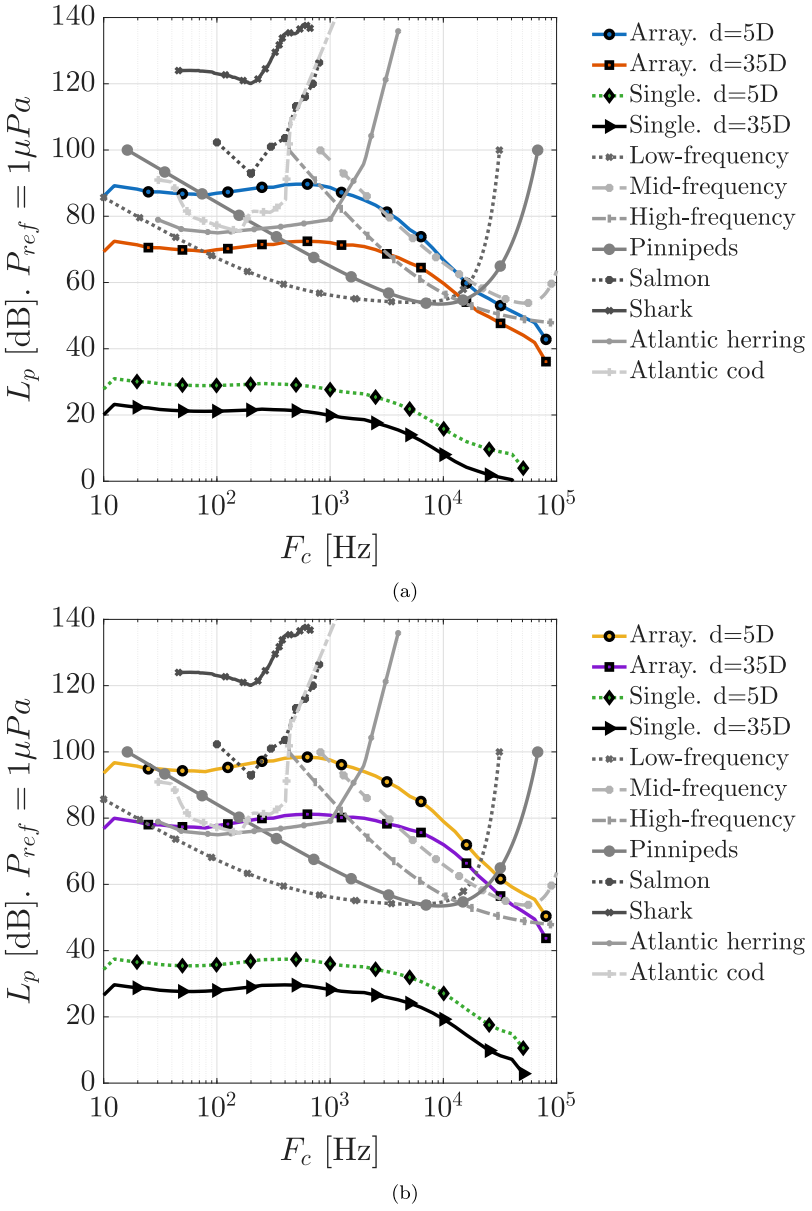

Fig. 10. Tidal array: noise of a rectangular layout of nine turbines evaluated at a distance d perpendicular to the inflow measured from the last central turbine (Fig. 1). (a) TSR = 4.0 and (b) TSR = 6.0.

The deployment of a nine-turbine tidal array has a pronounced impact on lateral observers. At TSR = 4.0, most marine species are affected at distances of up to $30D$, with the exception of sharks, salmon and high-frequency cetaceans. However, when the TSR increases to 6.0, the noise levels rise sufficiently to exceed the thresholds of salmon and high-frequency cetaceans, resulting in detectable impacts even at $30D$ distance.

4. Conclusions

We have presented a high-fidelity numerical framework that predicts the underwater noise of single and arrays of tidal-stream turbines by coupling turbulence-resolving flow simulations using the actuator-line method with semi-analytical acoustic theory. Applied to a full-scale 1 MW, 18-m diameter device, the framework provides new insight into how that turbine operation can generate sound levels above auditory thresholds of several marine species, including Atlantic cod, herring and low- and high-frequency cetaceans, over distances exceeding 1800 m. In contrast, species such as sharks and salmon appear to be less affected, with detectable responses only when the turbine operates at high tip-speed ratios and at a close range. These results outline that turbine design and operation strongly influence the scale and severity of acoustic impacts.

Environmental conditions further modulate these outcomes. Moderate levels of inflow turbulence substantially enhance leading-edge noise, extending the affected frequency range across both the low and high bands. This highlights the importance of site-specific hydrodynamic conditions in determining acoustic footprints. Beyond single devices, small arrays amplify and broaden noise emissions: our analysis of an idealized 3 × 3 layout shows increases of up to 8 dB downstream and 50 dB laterally, with mid-frequency cetaceans, otherwise unaffected by a single turbine, being exposed at distances of tens to hundreds of meters. In the present study, the acoustic impact of the array is estimated by assuming independent acoustic contributions from each turbine, which are superposed at the observer location.

This represents a first-order approximation that does not account for wake-induced modifications of the local inflow conditions, such as velocity deficit or changes in turbulence intensity, which could alter the apparent velocity and angle of attack experienced by downstream turbines.

The present analysis focuses on turbulence–interaction and trailing-edge noise as the dominant hydrodynamic noise sources of tidal turbines, as these mechanisms are typically the most significant for rotating blades operating with an attached turbulent boundary layer, which is the design condition of tidal turbines during normal operation. Other potential sources, such as mechanical noise, blade–tower interactions, and additional hydrodynamic mechanisms (e.g., tip-vortex noise, separation/stall noise, and blunt trailing-edge noise), are not included in the present framework. These mechanisms would contribute in addition to the noise sources modeled here and may therefore increase the total radiated sound levels. Consequently, the predicted sound levels should be interpreted as a lower-bound estimate of the total acoustic emissions that may occur during turbine operation. The long lifetime of tidal turbines, which are designed to operate continuously for 20–25 years, contrasts with the transient noise of ships or construction activities, raising particular concern about sustained exposure to marine fauna. While the results provide insight into the spatial scale at which turbine noise may exceed auditory thresholds of marine species, a comprehensive environmental impact assessment requires additional biological exposure metrics, such as temporary and permanent threshold shifts (TTS and PTS), as well as cumulative exposure considerations.

In the future, effective management will require collaboration between disciplines. Acoustic modelers, marine biologists, and policy makers must work together to define disturbance thresholds, establish monitoring protocols, and design marine spatial planning strategies that mitigate ecological risks. The modeling framework presented here can support these efforts by providing rapid estimates of turbine noise emissions that may serve as input for broader environmental assessments when combined with biological exposure metrics and site-specific studies. By integrating quantitative noise assessment into the development process, tidal energy can expand as a renewable resource while minimizing unintended impacts on marine ecosystems.

CRediT authorship contribution statement

Laura Botero-Bolívar: Writing – original draft, Visualization, Validation, Software, Methodology, Investigation, Funding acquisition, Formal analysis, Data curation, Conceptualization. **Pablo Ouro:** Writing – review & editing, Validation, Project administration, Methodology, Investigation, Funding acquisition, Formal analysis, Data curation. **Esteban Ferrer:** Writing – review & editing, Supervision, Project administration, Investigation, Funding acquisition, Formal analysis, Conceptualization.

Declaration of competing interest

The authors declare the following financial interests/personal relationships which may be considered as potential competing interests: Laura Botero-Bolivar reports financial support was provided by Industrial University of Santander. Esteban Ferrer reports financial support was provided by European Research Council. Pablo Ouro reports financial support was provided by Spanish Ministry of Science, Innovation and Universities (MCIU) and the State Research Agency (AEI). Pablo Ouro reports financial support was provided by UK Turbulence Consortium. If there are other authors, they declare that they have no known competing financial interests or personal relationships that could have appeared to influence the work reported in this paper.

Acknowledgments

This research has received funding from the European Union (ERC, Off-coustics, project number 101086075), from the grant number RYC2023-043451-I from the MCIU/AEI/10.13039/501100011033, Spain, and from Universidad Industrial de Santander, Colombia (project number 4632, "METODOLOGÍA DE PREDICCIÓN RÁPIDA DEL RUIDO SUBMARINO EN TURBINAS EÓLICAS Y MAREOMOTRICES Y SUS ARREGLOS"). Simulations have been performed using the Computer Shared Facilities (CSF) from the University of Manchester and the ARCHER2 UK National Supercomputing Service (https://www.archer2.ac.uk), partly supported by the UK Turbulence Consortium (UKTC) under EPSRC, UK grant no. EP/R029326/1. Views and opinions expressed are, however, those of the authors only and do not necessarily reflect those of the European Union or the European Research Council. Neither the European Union nor the granting authority can be held responsible for them.

Appendix A. Data: tidal turbine geometry

Table A.1 shows the geometry characteristics of the tidal turbine, where r is the radius location, c is the chord length, t is the airfoil thickness as a ratio of the chord length, and β is the twist angle.

Appendix B. Numerical simulation validation

The predicted power and thrust coefficient (C_P and C_T, respectively) by the LES–ALM code at four tip-speed ratios is provided in Fig. B.11, including in-house BEMT results and those from Scarlett et al. (2019). Two grid resolutions are provided, namely $\Delta x = 0.32$ m that is used for the noise prediction and a coarser resolution at 0.40 m. Values of C_P and C_T predicted from the LES–ALM do not vary depending on the grid resolutions adopted, with some slight larger values at TSR = 6, which agrees with previous observations from LES–ALM seen in other studies, e.g. Willden et al. (2023).

Data availability

The datasets generated and/or analyzed during the current study are available from the corresponding author upon reasonable request.

Table A.1
Geometry characteristics of the tidal turbine.

r [m]	c [m]	t [–]	β [°]	Hydrofoil
1.25	1.075	0.258	0.5672	NREL-S814
1.6375	1.285	0.3084	0.489556	NREL-S815
2.025	1.495	0.3588	0.4119	NREL-S816
2.4125	1.4227	0.341448	0.3528	NREL-S817
2.8	1.3211	0.317064	0.3061	NREL-S818
3.1875	1.2265	0.29436	0.2672	NREL-S819
3.575	1.1355	0.27252	0.2347	NREL-S820
3.9625	1.0547	0.253128	0.2068	NREL-S821
4.35	0.9843	0.236232	0.1841	NREL-S822
4.7375	0.9195	0.22068	0.1643	NREL-S823
5.125	0.8611	0.206664	0.1468	NREL-S824
5.5125	0.811	0.19464	0.1313	NREL-S825
5.9	0.7647	0.183528	0.1171	NREL-S826
6.2875	0.722	0.17328	0.1055	NREL-S827
6.675	0.685	0.1644	0.0955	NREL-S828
7.0625	0.651	0.15624	0.0853	NREL-S829
7.45	0.62	0.1488	0.0768	NREL-S830
7.8375	0.5922	0.142128	0.06932	NREL-S831
8.225	0.566	0.13584	0.06164	NREL-S832
8.6125	0.5417	0.130008	0.055487	NREL-S833

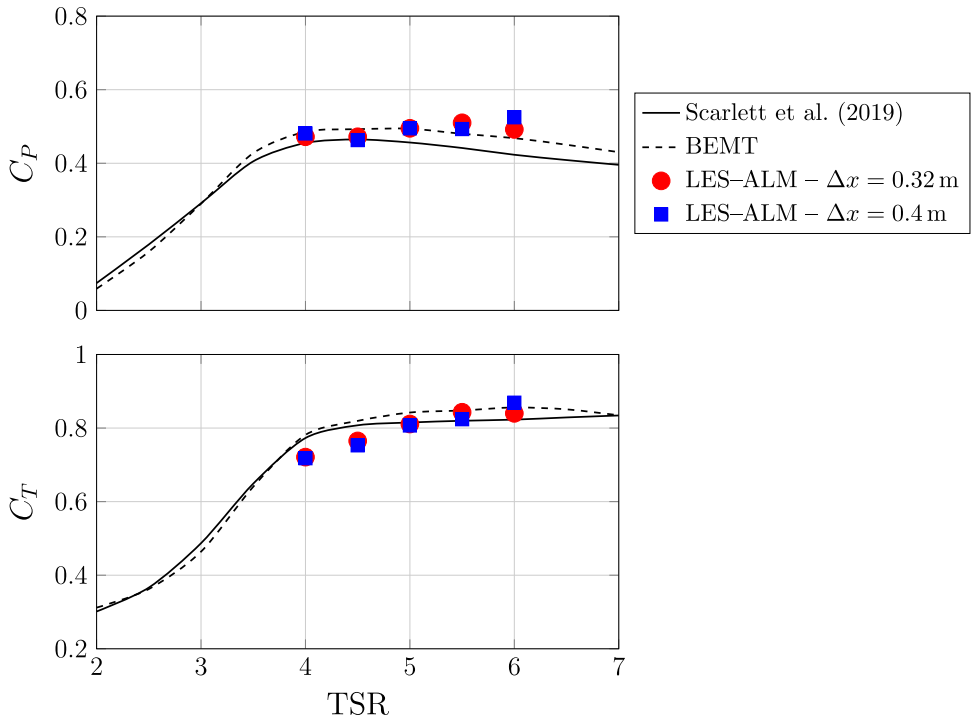

Fig. B.11. Power coefficient C_P (top) and thrust coefficient C_T (bottom) as a function of tip speed ratio (TSR). Solid line: Scarlett et al. (2019); dashed line: BEMT; filled circles: LES–ALM $\Delta x = 0.32\,\mathrm{m}$; filled squares: LES–ALM $\Delta x = 0.4\,\mathrm{m}$.

References

Afgan, I., McNaughton, J., Rolfo, S., Apsely, D., Stallard, T., Stansby, P.K., 2013. Turbulent flow and loading on a tidal stream turbine by LES and RANS. Int. J. Heat Fluid Flow 43, 96–108. http://dx.doi.org/10.1016/j.ijheatfluidflow.2013.03.010.

Ahmed, U., Apsley, D., Afgan, I., Stallard, T., Stansby, P.K., 2017. Fluctuating loads on a tidal turbine due to velocity shear and turbulence: Comparison of CFD with field data. Renew. Energy 112, 235–246. http://dx.doi.org/10.1016/j.renene.2017.05.048.

Amiet, R., 1975. Acoustic radiation from an airfoil in a turbulent stream. J. Sound Vib. 41 (4), 407–420. http://dx.doi.org/10.1016/S0022-460X(75)80105-2.

Amiet, R., 1976. Noise due to turbulent flow past a trailing edge. J. Sound Vib. 47 (3), 387–393. http://dx.doi.org/10.1016/0022-460X(76)90948-2.

Botero-Bolívar, L., dos Santos, F.L., Venner, C.H., de Santana, L.D., 2023. Experimental and predicted leading- and trailing-edge noise of symmetric airfoils under zero mean-loading. Appl. Acoust. 212, 1–14. http://dx.doi.org/10.1016/j.apacoust.2023.109579.

Botero-Bolívar, L., Marino, O.A., Venner, C.H., de Santana, L.D., Ferrer, E., 2024. Low-cost wind turbine aeroacoustic predictions using actuator lines. Renew. Energy 227, 120476. http://dx.doi.org/10.1016/j.renene.2024.120476.

Chawdhary, S., Angelidis, D., Colby, J., Corren, D., Shen, L., Sotiropoulos, F., 2018. Multi-resolution large-eddy simulation of an array of hydrokinetic turbines in a field-scale river: The Roosevelt Island Tidal Energy project in New York City. ArXiv Preprint.

Choi, W.-S., Hong, S.-Y., Song, J.-H., Kwon, H.-W., Park, I.-R., Seol, H.-S., Kim, M.-J., 2021. Time domain broadband noise predictions for non-cavitating marine propellers with wall pressure spectrum models. Int. J. Nav. Archit. Ocean. Eng. 13, 75–85. http://dx.doi.org/10.1016/j.ijnaoe.2021.01.004.

Christou, A., Stagonas, D., Buldakov, E., Stoesser, T., 2025. Focused waves on shear currents interacting with a vertical cylinder. Coast. Eng. 198, 104698. http://dx.doi.org/10.1016/j.coastaleng.2025.104698.

Churchfield, M.J., Li, Y., Moriarty, P.J., 2013. A large-eddy simulation study of wake propagation and power production in an array of tidal-current turbines. Philos. Trans. R. Soc. A: Math. Phys. Eng. Sci. 371 (1985), 20120421. http://dx.doi.org/10.1098/rsta.2012.0421.

Coles, D., Angeloudis, A., Greaves, D., Hastie, G., Lewis, M., Mackie, L., McNaughton, J., Miles, J., Neill, S., Piggott, M., Risch, D., Scott, B., Sparling, C., Stallard, T., Thies, P., Walker, S., White, D., Willden, R., Williamson, B., 2021. A review of the UK and British Channel Islands practical tidal stream energy resource. Proc. R. Soc. A 477, 20210469. http://dx.doi.org/10.1098/rspa.2021.0469.

Corcos, G., 1964. The structure of the turbulent pressure field in boundary-layer flows. J. Fluid Mech. 18 (3), 353–378. http://dx.doi.org/10.1017/S002211206400026X, Cited by: 556.

Dos Santos, F.L., 2023. Broadband Flow-Induced Noise for Airfoils: Inflow Turbulence Distortion Effect on Leading-Edge Noise Generation and Prediction (Ph.D. thesis). University of Twente.

Drela, M., 1989. XFOIL: An analysis and design system for low Reynolds number airfoils. Low Reynolds Number Aerodyn. 54, 1–12. http://dx.doi.org/10.1007/978-3-642-84010-4_1.

Enger, P.S., 1967. Hearing in herring. Comp. Biochem. Physiol. 22 (2), 527–538.

Erbe, C., Thomas, J.A., 2022. Exploring animal behavior through sound: Volume. Springer Nat. Gewerbestrasse (Switzerland) http://dx.doi.org/10.1007/978-3-030-97540-1.

Fisher, F.H., Simmons, V.P., 1977. Sound absorption in sea water. J. Acoust. Soc. Am. 62 (3), 558–564. http://dx.doi.org/10.1121/1.381574.

Garcia Novo, P., Kyozuka, Y., 2019. Analysis of turbulence and extreme current velocity values in a tidal channel. J. Mar. Sci. Technol. 24 (3), 659–672. http://dx.doi.org/10.1007/s00773-018-0601-z.

Ghobrial, M., Stallard, T., Schultz, D., Ouro, P., 2025. Evaluation of six subgrid-scale models for LES of wind farms in stable and conventionally-neutral atmospheric stratification. Bound.-Layer Meteorol. 191, 19. http://dx.doi.org/10.1007/s10546-025-00907-.

Gillespie, D., Palmer, L., Macaulay, J., Sparling, C., Hastie, G., 2021. Harbour porpoises exhibit localized evasion of a tidal turbine. Aquat. Conserv.: Mar. Freshw. Ecosyst. 31 (9), 2459–2468.

Go, S.T., Kingan, M.J., McKay, R.S., Sharma, R.N., 2023. Turbulent inflow noise produced by a shrouded propeller. J. Sound Vib. 542, 117366. http://dx.doi.org/10.1016/j.jsv.2022.117366.

Hansen, C.H., Doolan, C.J., Hansen, K.L., 2017. Wind Farm Noise: Measurement, Assessment, and Control. John Wiley & Sons.

Harding, H., Bruintjes, R., Radford, A.N., Simpson, S.D., 2016. Measurement of Hearing in the Atlantic Salmon (Salmo salar) Using Auditory Evoked Potentials, and Effects of Pile Driving Playback on Salmon Behaviour and Physiology. Marine Scotland Science.

Hasselman, D., Hemery, L., Copping, A., Fulton, E., Fox, J., Gill, A., Polagye, B., 2023. 'Scaling up' our understanding of environmental effects of marine renewable energy development from single devices to large-scale commercial arrays. Sci. Total Environ. 904, 166801.

Hastie, G., Russell, D., Lepper, P., Elliott, J., Wilson, B., Benjamins, S., Thompson, D., 2018. Harbour seals avoid tidal turbine noise: Implications for collision risk. J. Appl. Ecol. 55 (1), 334–344. http://dx.doi.org/10.1111/1365-2664.12981.

Hawkins, A.D., Popper, A.N., 2020. Sound detection by Atlantic cod: An overview. J. Acoust. Soc. Am. 148 (5), 3027–3041. http://dx.doi.org/10.1121/10.0002363.

Haxel, J., Zang, X., Martinez, J., Polagye, B., Staines, G., Deng, Z.D., Wosnik, M., O'Byrne, P., 2022. Underwater noise measurements around a tidal turbine in a busy port setting. J. Mar. Sci. Eng. 10 (5), 632. http://dx.doi.org/10.3390/jmse10050632.

Hemery, L., Garavelli, L., Copping, A., Farr, H., Jones, K., Baker-Horne, N., Kregting, L., McGarry, L., Sparling, C., Verling, E., 2024. Animal displacement from marine energy development: Mechanisms and consequences. Sci. Total Environ. 917, 170390.

Hildebrand, J.A., 2009. Anthropogenic and natural sources of ambient noise in the ocean. Mar. Ecol. Prog. Ser. 395, 5–20. http://dx.doi.org/10.3354/meps08353.

Hurubi, S., Ouro, P., Stansby, P., Stallard, T., 2025. Influence of seabed irregularity on the wake of a tidal turbine. Phys. Fluids 37, 075192.

Kim, S., Kinnas, S.A., 2022. Numerical prediction of propeller-induced noise in open water and ship behind conditions. Ocean Eng. 261, 112122. http://dx.doi.org/10.1016/j.oceaneng.2022.112122.

Lieber, L., Fraser, S., Coles, D., Nimmo-Smith, W.A.M., 2024. Sheared turbulent flows and wake dynamics of an idled floating tidal turbine. Nat. Commun. 15, 8244. http://dx.doi.org/10.1038/s41467-024-52578-x.

Liu, Y., Tang, Z., Huang, L., Stoesser, T., Fang, H., 2024. On the role of the froude number on flow, turbulence, and hyporheic exchange in open-channel flow through boulder arrays. Phys. Fluids 36 (9), http://dx.doi.org/10.1063/5.0222673.

Lloyd, T.P., Turnock, S.R., Humphrey, V.F., 2014. Assessing the influence of inflow turbulence on noise and performance of a tidal turbine using large eddy simulations. Renew. Energy 71, 742–754. http://dx.doi.org/10.1016/j.renene.2014.06.011.

Lossent, J., Lejart, M., Folegot, T., Clorennec, D., Di Iorio, L., Gervaise, C., 2018. Underwater operational noise level emitted by a tidal current turbine and its potential impact on marine fauna. Marine Poll. Bull. 131, 323–334. http://dx.doi.org/10.1016/j.marpolbul.2018.03.024.

Milne, I., Day, A., Sharma, R., Flay, R., 2016. The characterisation of the hydrodynamic loads on tidal turbines due to turbulence. Renew. Sustain. Energy Rev. 56, 851–864. http://dx.doi.org/10.1016/j.rser.2015.11.095.

Mycek, P., Gaurier, B., Germain, G., Pinon, G., Rivoalen, E., 2014. Experimental study of the turbulence intensity effects on marine current turbines behaviour. Part I: One single turbine. Renew. Energy 66, 729–746. http://dx.doi.org/10.1016/j.renene.2013.12.036.

Nicoud, F., Ducros, F., 1999. Subgrid-scale stress modelling based on the square of the velocity gradient tensor. Flow, Turbul. Combust. 62 (3), 183–200. http://dx.doi.org/10.1023/A:1009995426001.

Nieder, C., 2023. Comparative Hearing Abilities in Sharks (Ph.D. thesis). University of Auckland.

Nigro, D., Abrahams, I.D., 2016. On trailing edge noise with application in hydroacoustics. In: 22nd AIAA/CEAS Aeroacoustics Conference. p. 2870.

Ouro, P., Fernández, R., Armstrong, A., Brooks, B., Burton, R.R., Folkard, A., Ilic, S., Parkes, B., Schultz, D.M., Stallard, T., Watson, F.M., 2024a. Environmental impacts from large-scale offshore renewable-energy deployment. Environ. Res. Lett. 19, 063001. http://dx.doi.org/10.1088/1748-9326/ad4c7d.

Ouro, P., Harrold, M., Stoesser, T., Bromley, P., 2017. Hydrodynamic loadings on a horizontal axis tidal turbine prototype. J. Fluids Struct. 71, 78–95. http://dx.doi.org/10.1016/j.jfluidstructs.2017.03.009.

Ouro, P., Mullings, H., Christou, A., Draycott, S., Stallard, T., 2024b. Wake characteristics behind a tidal turbine with surface waves in turbulent flow analyzed with large-eddy simulation. Phys. Rev. Fluids 9 (3), 034608. http://dx.doi.org/10.1103/PhysRevFluids.9.034608.

Ouro, P., Nishino, T., 2021. Performance and wake characteristics of tidal turbines in an infinitely large array. J. Fluid Mech. 925, A30. http://dx.doi.org/10.1017/jfm.2021.692.

Ouro, P., Ramírez, L., Harrold, M., 2019. Analysis of array spacing on tidal stream turbine farm performance using Large-Eddy Simulation. J. Fluids Struct. 91, 102732. http://dx.doi.org/10.1016/j.jfluidstructs.2019.102732.

Ouro, P., Stansby, P., Macleod, A., Stallard, T., Mullings, H., 2023. High-fidelity modelling of a six-turbine tidal array in the shetlands. In: 15th European Wave and Tidal Energy Conference 442, Vol. 15. Sep. 2023, http://dx.doi.org/10.36688/ewtec-2023-442.

Ouro, P., Stansby, P.K., Stallard, T., 2022. Analysis of the kinetic energy recovery behind a tidal stream turbine for various submergence levels. Int. Mar. Energy J. 5 (3), 265–272. http://dx.doi.org/10.36688/imej.5.265-272.

Ouro, P., Stoesser, T., 2019. Impact of environmental turbulence on the performance and loadings of a tidal stream turbine. Flow, Turbul. Combust. 102 (3), 613–639. http://dx.doi.org/10.1007/s10494-018-9975-6.

Palmer, L., Gillespie, D., Macaulay, J., Sparling, C., Russell, D., Hastie, G., 2021. Harbour porpoise (*Phocoena phocoena*) presence is reduced during tidal turbine operation. Aquat. Conserv.: Mar. Freshw. Ecosyst. 31 (12), 3543–3553. http://dx.doi.org/10.1002/aqc.3737.

Pine, M.K., Schmitt, P., Culloch, R., Lieber, L., Kregting, L., 2019. Providing ecological context to anthropogenic subsea noise: Assessing listening space reductions of marine mammals from tidal energy devices. Renew. Sustain. Energy Rev. 103, 49–57. http://dx.doi.org/10.1016/j.rser.2018.12.024.

Posa, A., Broglia, R., 2021. Momentum recovery downstream of an axial-flow hydrokinetic turbine. Renew. Energy 170, 1275–1291. http://dx.doi.org/10.1016/j.renene.2021.02.061.

Posa, A., Viola, I.M., Broglia, R., 2024. Influence of the tip speed ratio on the wake dynamics and recovery of axial-flow turbines. Phys. Fluids 36 (5), http://dx.doi.org/10.1063/5.0203285.

Purser, J., Radford, A.N., 2011. Acoustic noise induces attention shifts and reduces foraging performance in three-spined sticklebacks (Gasterosteus aculeatus). PLoS ONE 6 (2), e17478. http://dx.doi.org/10.1371/journal.pone.0017478.

Risch, D., van Geel, N., Gillespie, D., Wilson, B., 2020. Characterisation of underwater operational sound of a tidal stream turbine. J. Acoust. Soc. Am. 147 (4), 2547. http://dx.doi.org/10.1121/10.0001124.

Scarlett, G., Sellar, B., van den Bremer, T., Viola, I., 2019. Unsteady hydrodynamics of a full-scale tidal turbine operating in large wave conditions. Renew. Energy 143 (2), 199–213.

Schlinker, R.H., Amiet, P.E., 1963. On the noise generated by an airfoil trailing edge in a turbulent stream. J. Acoust. Soc. Am. 37 (5), 1015–1022. http://dx.doi.org/10.1121/1.1918617.

Schlinker, R., Amiet, R., 1981. Helicopter rotor trailing edge noise. In: 7th Aeroacoustics Conference. p. 2001.

Sellar, B.G., Wakelam, G., Sutherland, D.R.J., Ingram, D., Venugopal, V., 2018. Characterisation of tidal flows at the European marine energy centre in the absence of ocean waves. Energies 11, 176. http://dx.doi.org/10.3390/en11010176.

Shen, W.Z., Sørensen, J.N., Mikkelsen, R., 2005. Tip loss correction for actuator/Navier–Stokes computations. J. Sol. Energy Eng. 127 (2), 209–213. http://dx.doi.org/10.1115/1.1850488.

Southall, B.L., Finneran, J.J., Reichmuth, C., Nachtigall, P.E., Ketten, D.R., Bowles, A.E., Ellison, W.T., Nowacek, D.P., Tyack, P.L., 2019. Marine mammal noise exposure criteria: updated scientific recommendations for residual hearing effects. Aquatic Mammals 45 (2), 125–232. http://dx.doi.org/10.1578/AM.45.2.2019.125.

Sparling, C., Lonergan, M., McConnel, B., 2018. Harbour seals (Phoca vitulina) around an operational tidal turbine in Strangford Narrows: No barrier effect but small changes in transit behaviour. Aquat. Conserv.: Mar. Freshw. Ecosyst. 28 (1), 194–204.

Tougaard, J., 2021. Thresholds for noise induced hearing loss in marine mammals. Sci. Note DCE – Dan. Cent. Environ. Energy 118, 3154–3163.

Troldborg, N., Larsen, G.C., Madsen, H.A., Hansen, K.S., Sørensen, J.N., Mikkelsen, R., 2011. Numerical simulations of wake interaction between two wind turbines at various inflow conditions. Wind. Energy 14 (7), 859–876. http://dx.doi.org/10.1002/we.433.

United States. National Marine Fisheries Service. Office of Protected Resources, 2024. 2024 Update to: Technical Guidance for Assessing the Effects of Anthropogenic Sound on Marine Mammal Hearing (Version 3.0): Underwater and In-Air Criteria for Onset of Auditory Injury and Temporary Threshold Shifts. Technical Report, National Oceanic and Atmospheric Administration.

Willden, R., Chen, X., Harvey, S.T., Edwards, H., Vogel, C., Bhavsar, K., Allsop, T., Gilbert, J., Mullings, H., Ghobrial, M., Ouro, P., Apsley, D., Stallard, T., Benson, I., Young, A., Schmitt, P., de Arcos, F.Z., Dufour, M.-A., Bex, C.C., Pinon, G., Evans, A., Togneri, M., Masters, I., da Silva Ignacio, L., Duarte, C., Souza, F., Gambuzza, S., Liu, Y., Viola, I.M., Rentschler, M., Gomes, T., Vaz, G., Azcueta, R., Ward, H., Salvatore, F., Sarichloo, Z., Calcagni, D., Tran, T.T., Ross, H., Oliveira, M., Puraca, R., Carmo, B., 2023. Tidal turbine benchmarking project: Stage I - Steady flow blind predictions. In: Proceedings of the 15th European Wave and Tidal Energy Conference. http://dx.doi.org/10.36688/ewtec-2023-574.

Zilic de Arcos, F., Vogel, C.R., Willden, R.H., 2023. A numerical study on the hydrodynamics of a floating tidal rotor under the combined effects of currents and waves. Ocean Eng. 286, 115612. http://dx.doi.org/10.1016/j.oceaneng.2023.115612.